



Metacaspase MC1 enhances aluminum-induced programmed cell death of root tip cells in Peanut

Shaochang Yao · Shuzhen Luo · Chunliu Pan ·
Weijiao Xiong · Dong Xiao · Aiqin Wang · Jie Zhan ·
Longfei He

Received: 9 December 2019 / Accepted: 2 February 2020 / Published online: 15 February 2020
© Springer Nature Switzerland AG 2020

Abstract

Aims Metacaspases are cysteine-dependent proteases, which play essential roles in programmed cell death (PCD), and caspase-3-like protease is the crucial executioner. However, its response mechanism to aluminum (Al)-induced PCD is still elusive.

Methods Here, the type I metacaspase gene in peanut (*Arachis hypogaea* L.), *AhMC1*, was cloned from the Al-sensitive cultivar ZH2. Physiological and biochemical methods, as well as gene expression analyses, were employed to explore its function in Al-induced PCD in peanut root tips.

Results *AhMC1* had a 1068-bp open reading frame, encoding a peptide of 355 amino acids, and the purified protein exhibited a high caspase-3-like protease activity. Its expression levels in different tissues of peanut varieties ZH2 and 99–1507 (Al-tolerant) varied under Al-

stress conditions. The subcellular localization indicated that *AhMC1* was transferred from mitochondria into the cytoplasm. Furthermore, overexpressing *AhMC1* reduced the resistance to Al stress. Sense transgenic plants showed a low relative root growth rate, and reduced superoxide dismutase, peroxidase, and catalase activities, compared with wild-type and antisense transgenic plants under Al-stress conditions, but had a high root-cell death rate, and increased Al and maleic dialdehyde contents.

Conclusions The data suggest that metacaspase *AhMC1* is a positive factor in Al-induced PCD in peanut root tips.

Keywords Metacaspase · *AhMC1* · Aluminum toxicity · PCD · Peanut root tips

Shaochang Yao and Shuzhen Luo contributed equally to this work.

Responsible Editor: Juan Barcelo.

Electronic supplementary material The online version of this article (<https://doi.org/10.1007/s11104-020-04448-w>) contains supplementary material, which is available to authorized users.

S. Yao · S. Luo · C. Pan · W. Xiong · D. Xiao · A. Wang ·
J. Zhan · L. He
College of Agronomy, Guangxi University, Nanning, Guangxi,
China

S. Yao
College of Pharmacy, Guangxi University of Chinese Medicine,
Nanning, Guangxi, China

S. Yao · C. Pan
College of Life Science and Technology, Guangxi University,
Nanning, Guangxi, China

D. Xiao · A. Wang · J. Zhan (✉) · L. He (✉)
Guangxi Key Laboratory for Agro-Environment and
Agro-Product Safety, Nanning, Guangxi, China
e-mail: may2399@163.com
e-mail: lfhe@gxu.edu.cn

Abbreviations

Al	Aluminum
AT	Antisense transgenic
CAT	Catalase
MC	Metacaspase
MDA	Maleic dialdehyde
PCD	Programmed cell death
POD	Peroxidase
RACE	Rapid amplification of cDNA ends
ROS	Reactive oxygen species
SOD	Superoxide dismutase
ST	Sense transgenic
WT	Wild-type

Introduction

Aluminum (Al) is an abundant metal on the earth's surface, constituting approximately 7% metal content, and its toxicity is a major restrictive factor for crop growth in acidic soils, especially in southern China. Once the soil pH < 5.0, Al³⁺ is easily dissolved, resulting in the inhibition of plant root elongation and induced appearance of programmed cell death (PCD) (Huang et al. 2014a; Zhan et al. 2013). PCD is genetically controlled cell death that is activated in response to environmental stresses in plants. The important role of caspases in regulating apoptosis in animals strongly influenced research on PCD in plants, resulting in many caspase-like activities being detected in plants (Acosta-Maspons et al. 2014; Coll et al. 2010; Lam and Zhang 2012). However, instead of caspases, metacaspases (caspase-like proteins, MCs) are involved in PCD events in plants (Fagundes et al. 2015; Minina et al. 2014).

Plant MCs are divided into two types, I and II, on the basis of their structure, with the former having an N-terminal prodomain that is not present in the latter (Choi and Berges 2013; Fagundes et al. 2015; Lam and Zhang 2012; Tsiatsiani et al. 2011). Evidence suggests that MCs are involved in signaling, developmental regulation and stress-induced PCD of plants (Fagundes et al. 2015; Huang et al. 2015; Lam and Zhang 2012). Several MC genes have been identified and play crucial roles in plant PCD. For example, in *Arabidopsis thaliana*, three type I (*AtMC1–3*) and six type II (*AtMC4–9*) genes have been identified (Tsiatsiani et al. 2011). *AtMC1* and *AtMC2* antagonistically control hypersensitive response-triggered PCD (Coll et al. 2010). *AtMC1* is a positive regulator of cell death and depends on the

conserved catalytic residues, whereas *AtMC2* negatively regulates cell death and is independent of the catalytic residues (Coll et al. 2010). *AtSERPIN1* is an inhibitor of *AtMC1*-mediated cell death and autocatalytic processing in planta (Lema Asqui et al. 2017).

Among the type II MCs, *AtMC4* is a positive regulator of the biotic and abiotic stress-induced PCD in *Arabidopsis* (Watanabe and Lam 2011). *AtMC5* mediates apoptosis triggered by oxidative stress or aging in yeast (Watanabe and Lam 2005). *AtMC8*'s expression is strongly upregulated by the oxidative stresses of UVC and H₂O₂ (He et al. 2008). *AtMC9* is required for the efficient progression of autolysis in xylem cell death (Bollhoner et al. 2013; Escamez et al. 2016) and PCD in leaves (Wrzaczek et al. 2015). Additionally, the *mcII* gene in Norway spruce (Bozhkov et al. 2005), *MC4* in wheat (Wang et al. 2012), *MC9* in pepper (Kim et al. 2013), *NbMCA1* in tobacco (Hao et al. 2007) and *MCII-1* in litchi (Wang et al. 2017a) also appear to function in PCD and defense responses.

Recently, MC genes have been systematically predicted and identified through genome-wide screening, including in rubber tree (Liu et al. 2016a), grape (Zhang et al. 2013), rice (Wang and Zhang 2014), maize (Ahmad et al. 2012), and tomato (Hoeberichts et al. 2003; Liu et al. 2016b). Thus, MCs are vital regulators of plant PCD. However, to date, no MC genes have been reported in peanut.

Peanut, as an important oil crop worldwide, is mostly planted in acidic soils in China, especially in southern China. A negative correlation between Al-triggered PCD and tolerance to Al exists in peanut (Zhan et al. 2013). Different types of caspase-like proteases are activated in root tips of peanut during Al-induced PCD, and caspase-3-like protease is a crucial executioner (Huang et al. 2014b; Yao et al. 2016). MC proteases having caspase-3-like abilities have also been identified in *Papaver rhoeas*, *Arabidopsis* and poppy (Chai et al. 2017; Tan et al. 2016; Wilkins et al. 2015). In this study, we report that *AhMC1*, a type I MC, enhances Al-induced PCD in peanut root tips.

Materials and methods

Plant material and treatment

Plant preparation and treatment were performed as described by Yao et al. (2016) with slight modifications.

Seeds of peanut cultivars Zhonghua 2 (ZH2, Al-sensitive) and 99–1507 (Al-tolerant) were incubated in wet perlite under dark conditions at 26 ± 2 °C for approximately 3 d to germinate. Seedlings were cultured in Hoagland's nutrient solution (pH 4.2) under a 12-h light period with a photon flux density of $30\text{--}50 \mu\text{mol m}^{-2} \text{s}^{-1}$ from daylight fluorescent tubes (Philips Chinese Ltd., Shanghai, China) at 26 ± 2 °C when the seedlings had 2-cm long roots (1 d after germination). When the third leaves emerged, the seedlings were pretreated in Hoagland's nutrient solution supplemented with 0.1 mM CaCl_2 (pH 4.2) for 24 h.

For gene cloning, ZH2 seedlings were transferred to fresh Hoagland's nutrient solution supplemented with 100 μM AlCl_3 for 12 h, and approximately 1 cm root tips were removed and placed on filter paper. For real-time quantitative (RT-q) PCR and western blot analyses, leaves, stems, and root tips of the two cultivars were sampled at 0, 4, 8, 12, and 24 h during the 100- μM AlCl_3 treatment, and plants not receiving the Al treatment were used as the controls. Samples from all the experiments were immediately frozen in liquid nitrogen and stored at -80 °C until used for RNA and protein extractions. Leaves of tobacco (*Nicotiana tabacum* cv. K326) were decontaminated in 0.1% HgCl_2 (w/v) for 8 min, followed by 5% (v/v) detergent for 15–20 min, and running water for 30 min. Subsequently, a sample of 10 cm \times 20 cm was taken after four or five washes in sterile distilled water and cultured on Murashige and Skoog (MS) medium supplemented with 3% (w/v) sucrose, 0.5% (w/v) agar powder (gel strength: $>1400 \text{ g cm}^{-2}$), and 1.0 mg L^{-1} 6-Benzylaminopurine (6-BA) to induce cluster-buds. To obtain the seedlings, the cluster-buds were cultured in MS solid medium supplemented with 2.5 mg L^{-1} 6-BA and 0.5 mg L^{-1} 1-naphthylacetic acid (NAA), and subcultured for 20 d. The cultures were incubated at 26 ± 2 °C with a 16-h/8-h light/dark photoperiod. Leaves were used as explants for genetic transformations.

Cloning and structural analysis of *AhMCI*

Total RNA from ZH2 root tips was extracted using the TRIzol method (Catalog No. 15596–018; Invitrogen Life Technologies, Carlsbad, California, USA) as described in the manufacturer's instructions. A first-strand cDNA template for RACE-PCR amplification was synthesized according to the manufacturer's instructions (Catalog No. 1621, TaKaRa Bio, Dalian, China). All the primers for PCR amplification were designed using Primer Premier

5.0 software (Table S1) and amplified full-length cDNAs. Each PCR reaction was carried out in a 25- μL final volume, containing 12.5 μL Taq polymerase Master Mix, 1 μL first-strand cDNA (approximately 10 ng), 1 μL PCR primers and 9.5 μL ddH_2O . The reaction procedure is shown in Table S1. The 3'- and 5'-RACE reactions were performed using SMARTer® RACE 5'/3' Kit. The RACE-PCR products were purified using a Gel Extraction Kit (Catalog No. DP209, Tiangen Biotech, Beijing, China), and the amplified products were cloned into vector pMD19-T (Catalog No. D102A, TaKaRa Bio, Dalian, China). The resultant recombinant plasmid was transformed into *Escherichia coli* strain DH5 α and then sent to BGI Genomics Co., Ltd. (Shenzhen, China) for sequencing. The 3'- and 5'- termination fragments were spliced together using DNAMAN (Lynnon Biosoft, San Ramon, USA) to obtain the full-length *AhMCI* gene. All the sequences were analyzed based on non-redundant databases at NCBI (<http://www.ncbi.nlm.nih.gov/>) using BLAST. The theoretical molecular weight and isoelectric point of *AhMCI* protein were predicted by ExpAsy (http://web.expasy.org/compute_pi/). Conserved domains were analyzed using the conserved domain search service at the NCBI web (<http://www.ncbi.nlm.nih.gov/Structure/cdd/wrpsb.cgi>). The subcellular localization was predicted using PSORT prediction software (<http://psort.hgc.jp/form.html>). Transmembrane structures were analyzed using the TMHMM Server v.2.0 (<http://www.cbs.dtu.dk/services/TMHMM/>). Protein signal peptides were analyzed using the SignalP 4.1 server (<http://www.cbs.dtu.dk/services/SignalP/>). The sequence of *AhMCI* was uploaded to the NCBI GenBank database under accession number MN400565. The genomic DNA sequences of *AhMCI* were obtained through a BLASTN search of the genomic databases (<https://www.peanutbase.org/blast/>) of *Arachis duranensis* and *Arachis ipaensis*, which are the diploid ancestors of cultivated peanut (Bertioli et al. 2016), and verified by PCR. The exon–intron structure of *AhMCI* was identified using coding sequence alignments to corresponding genomic sequences.

Multiple sequence alignments and phylogenetic analysis

MEGA 6.0 (<http://www.megasoftware.net>) was used to conduct the phylogenetic analyses of the MCs and *AhMCI*. MC members used for the phylogenetic analysis were obtained from the GenBank (<https://www>.

ncbi.nlm.nih.gov/genbank/) and TAIR (<http://www.arabidopsis.org/>) databases. The amino acid sequences of 21 members were aligned using ClustalX 1.83 software, and the phylogenetic trees were constructed with the neighbor-joining approach. The bootstrap values, and gaps and missing data treatments, were set at 1000 replicates and complete deletion options, respectively.

The *MC* genes were named using the first letter of the genus followed by the first letter of the species. Members of *MCs* used for phylogenetic analysis were indicated as following: AtMC1, AT1G02170.1 (*A. thaliana*); AtMC2, AT4G25110; AtMC3, AT5G64240.2; AtMC4, AT1G79340.1; AtMC5, AT1G79330.1; AtMC6, AT1G79320.1; AtMC7, AT1G79310.1; AtMC8, AT1G16420.1; AtMC9, AT5G04200.1; VaMC3, XP_017408034.1 (*Vigna angularis*); AiMC1, XP_016179981.1 (*A. ipaensis*); AiMC3, XP_016180860.1; AdMC1, XP_015943473.1 (*A. duranensis*); LaMC3, XP_019426387.1 (*Lupinus angustifolius*); CaMC3, XP_004485587.1 (*Cicer arietinum*); GmMC1, KRH43894.1 (*Glycine max*); MtMC1, XP_003593211.1 (*Medicago truncatula*); VrMC3, XP_014519171.1 (*Vigna radiata* var. *radiata*); CcMC1, XP_020222169.1 (*Cajanus cajan*); and GsMC1, A0A0B2R4L3 (*Glycine soja*).

Real-time quantitative PCR analysis

RT-qPCR analyses of *AhMC1* expression in different tissues (leaves, stems, and roots) of peanut were performed with SYBR® Premix Ex Taq™ (Bio-Rad Laboratories, Hercules, CA, USA) using the CFX96™ Real-Time System, according to the supplier's manuals. The *UBQ10R* gene (accession number EG030441) (Table S2) was used as the internal control to quantify the relative transcript levels (Yao et al. 2019). The primers of *AhMC1* and *UBQ10R* are shown in Table S1. The reactions were prepared in a total volume of 20 μ L containing 10 μ L SYBR® Premix Ex Taq™, 2 μ L cDNA, 1 μ L each 10- μ M primer, and 6 μ L ddH₂O. The relative level of gene expression was calculated using the $2^{-\Delta\Delta C_t}$ formula. Three technical replicates were run for each biological sample.

Western blot analysis

Approximately 200 mg of peanut root tips were ground in liquid nitrogen and then transferred to 500 μ L protein lysis buffer (Catalog No. P0013B, Beyotime Institute of

Biotechnology, Shanghai, China) containing 50 mM Tris-HCl (pH 7.4), 0.15 M NaCl, 10% glycerol (w/v), 0.1% sodium dodecyl sulfate (SDS) (w/v), 1% TritonX-100 (w/v), 1% sodium deoxycholate (w/v) and 1 mM phenylmethanesulfonyl fluoride. The extracts were placed on ice for 20 min, followed by centrifugation at 12,000 \times g for 15 min at 4 °C. The supernatants were transferred to a fresh 1.5 mL tube and 6–10 times the volume of 1:1 acetone:alcohol (v/v) was added. Samples were centrifuged at 15,000 \times g for 10 min at 4 °C and then maintained at -20 °C for 1 h or overnight. The pellets were redissolved in 100 μ L lysis buffer after being air dried for 10 min. The lysates were either used immediately or stored at -80 °C. The protein concentrations were determined using an enhanced BCA protein assay kit (Catalog No. P0010S, Beyotime Institute of Biotechnology, Shanghai, China) according to the manufacturer's instructions.

For western blotting, equal amounts of lysates were mixed with 4 \times SDS-loading dyes treated for 10 min at 99 °C and electrophoresed in 12% SDS-polyacrylamide gels. The separated proteins were transferred to polyvinylidene fluoride membranes (Catalog No. IPVH00010, Millipore, Burlington, MA, USA) using a trans-blot cell (Bio-Rad) after electrophoresis. The membranes were blocked with 5% Difco™ Skim milk (Catalog No. D8340, Solarbio Science & Technology Co, Ltd., Beijing, China) at least 1.5 h. After washing three times with 1 \times TBS-T (Catalog No. T1081-500, Solarbio Science & Technology Co, Ltd., Beijing, China) for 5 min each, membranes were incubated with a polyclonal primary antibody to the whole *AhMC1* peptide produced by Ab-mart Company (Shanghai, China) at a 1:500 dilution overnight. After washing three times in the same washing buffer, for a total of 15 min, each membrane was incubated with a secondary rabbit anti-goat antibody conjugated with horseradish peroxidase conjugate (Catalog No. ZB-2306, ZSGB-Bio, Beijing, China) at a 1:5000 dilution at room temperature for 2 h. After several washes with the same washing buffer, 5 min each time, an ECL western blotting analysis system was used to detect the substrates using an ECL chemiluminescence kit (Catalog No. CW0049B, CWBio, Beijing, China) according to the manufacturer's instructions. The integrated optical densities (IODs) of the bands produced by western blotting were analyzed using Gel-pro Analyzer 4.0 software (Media Cybernetics, Bethesda, MD, USA) (Cheng et al. 2013). The relative IODs of the bands were calculated using the

ratios of the IOD of AhMC1 protease to the IOD of β -Actin protease.

Subcellular localization of AhMC1 determined by immune-electron microscopy

To investigate the ultrastructural localization and changes after Al treatments, the root tips of ZH2 were treated with 100 μ M $AlCl_3$ for 0, 4, 8, 12, and 24 h. The root tips (approximately 2 mm) were fixed in 100 mM phosphate buffer (pH 7.2) containing 4% methanol, and 0.5% glutaraldehyde for 2 h at 4 °C. The tissues were dehydrated in an ethanol series, permeated in a K_4M series at -20 °C and embedded in K_4M araldite resin. Ultrathin sections were cut with an LKB ultra microtome (8800, LKB, Bromma, Sweden) and collected on nickel grids for the immune colloidal gold technique.

Grid-mounted tissue sections were processed for colloidal gold immunocytochemistry by incubating the sections with primary antibody (1:100 dilution), and subsequently the immunolabeled patterns were visualized with a protein A-colloidal gold complex (14-nm gold particles). This was followed by conventional staining with 2% uranyl acetate in 50% methanol for 10 min and then lead citrate for 7 min. The sections were examined under a transmission electron microscope (JEM-1200EX, JEOL, Tokyo, Japan) operated at 80 KV.

Protein expression, purification and activity assay

Recombinant pET-15b-*AhMC1* was transformed into *E. coli* strain Rosetta (DE3) (Sangon Biotech Co., Ltd., Shanghai, China). The strain cells were cultured in LB liquid media supplemented with ampicillin (50 μ g mL^{-1}) and chloramphenicol (34 μ g mL^{-1}) at 37 °C with a shaking at 220 rpm for 2–3 h until the OD_{600} value reached 0.4–0.6. They were subsequently induced using 0.5 mM isopropyl- β -D-thiogalactoside at 25 °C overnight and then at 37 °C for 4 h with a shaking at 220 rpm. Subsequently, the cells were pelleted by centrifugation at 4000 $\times g$ for 10 min and resuspended in 500 μ L Tris-buffered saline (pH 7.4) containing 8 M urea, 50 mM Tris-HCl, and 300 mM NaCl. SDS-PAGE was performed, using 40 μ L supernatant mixed with 10 μ L 5 \times protein loading buffer treated for 10 min at 99 °C. After ultrasonication on ice for 20 min, the supernatant was collected by centrifugation at 12,000 $\times g$ for 20 min at 4 °C and then purified using Ni-NTA affinity chromatography as described by Wang

et al. (2017b). Purified AhMC1 was confirmed through western blotting experiments. Fluorogenic Ac-DEVD-pNA, as a substrate of caspase-3, was used to measure enzymatic activities as described previously (Yao et al. 2016).

Tobacco *AhMC1* transformation and transgenic plant confirmation

To investigate the roles of *AhMC1* in plants, transgenic tobacco plants were generated. The sense (ST) and transgenic genes were cloned using cDNA of ZH2 as the template and the primer pairs shown in Table S1. The genes were independently inserted into a pBI121-*eGFP* vector that contained green fluorescent protein (GFP), cauliflower mosaic virus 35S (CaMV35S) promoter and nopaline synthase terminator using *XhoI* and *SpeI* restriction sites to generate the recombination plasmids pBI121-*AhMC1-eGFP*. Subsequently, the recombinant plasmids were independently transformed into *N. tabacum* cv. K326 using an *Agrobacterium*-mediated transformation method. From 60 putative transgenic tobacco seedlings, 30 ST plants were propagated in selective MS culture medium supplemented with 0.5 mg L^{-1} 6-BA, 0.2 mg L^{-1} NAA, and 100 mg L^{-1} kanamycin (Kan), and rooted in 1/2 MS medium supplemented with 0.5 mg L^{-1} NAA and 100 mg L^{-1} Kan. The transgenic plants were produced using the leaf-disk infection method in a 100 mg L^{-1} Kan-selection culture. T1 seedlings were used for transgenic plant confirmation. The green fluorescence of *GFP* was detected using a confocal laser scanning microscope with excitation at 488 nm and emission capture at 500–550 nm. Simultaneously, genomic DNA was extracted from roots of transgenic T1 generations and wild-type (WT) tobacco plants using the cetyl trimethyl ammonium bromide method with a slight modification (Gilio et al. 2017). The specific primers used for PCR confirmation are shown in Table S1, and each PCR reaction was carried out in a final volume of 25 μ L, containing 12.5 μ L Taq polymerase Master Mix, 1 μ L first-strand cDNA (approximately 10 ng), 1 μ L PCR primers, and 9.5 μ L ddH_2O .

Assays of relative root growth, cell death and Al content in transgenic tobacco

The effects of different treatments on root growth, cell death and Al content were determined as described by

Yao et al. (2016) in two peanut cultivars. The relative root growth was determined by measuring the main root length, and the relative root elongation was calculated using the following formula: $(L_{24h} - L_{0h}) \times 100\% L_{0h}^{-1}$, where L_{24h} represents the root length after the 24-h AI treatment and L_{0h} represents the initial root length before the AI treatment.

Assay of caspase-3-like activities in transgenic tobacco

The caspase-3-like activity was determined as described by Yao et al. (2016). In brief, root tips (1.0 ± 0.1 cm) were homogenized in lysis buffer (approximately 100 μ L/3–10 mg sample). The homogenate was immediately collected by centrifugation at $12,000 \times g$ for 10 min at 4 °C. The supernatant was used for the reactions or stored at -80 °C. Caspase-3-like activities were detected using a 100- μ L reaction mixture containing 25 μ L extract, 5 μ L 2 mM caspase substrate, and 70 μ L caspase assay buffer, at 405 nm with a microplate reader (Tecan Infinite RF200 pro, Swiss) after incubation under continuous dark conditions at 37 °C for 2 h. The protein concentration of the extract was determined quantitatively using the Bradford assay.

RT-qPCR analysis of *AhMCI* in transgenic tobacco

The expression of *AhMCI* in the T1 generation of transgenic tobacco plants under AI stress was detected using RT-qPCR. *NtActin* transcripts (Table S1) were used as an internal control in tobacco K326 (Pena et al. 2017) to quantify *AhMCI* expression. The 35-cycle reaction was carried out in a total volume of 20 μ L, containing 10 μ L SYBR® Premix Ex Taq™, 2 μ L cDNA, 1 μ L of each 10 μ M primer, and 6 μ L ddH₂O. The RT-qPCR analysis method was the same as for *AhMCI* expression in peanut.

Assays of maleic dialdehyde (MDA), superoxide dismutase (SOD), peroxidase (POD), and catalase (CAT) activities in transgenic tobacco

MDA was measured using the thiobarbituric acid (TBA)-based colorimetric method as described by Phan et al. (2016). Superoxide dismutase (SOD), peroxidase (POD), and catalase (CAT) activities were determined as described by Pan et al. (2017). In brief, SOD activity was determined by measuring the inhibition of photochemical reduction of nitro-blue-tetrazolium at 560 nm,

and POD activity was determined by measuring the rate of guaiacol oxidation and monitoring the absorbance at 470 nm. CAT activity was determined by detecting the decomposition of H₂O₂ and monitoring the decrease in the absorbance at 240 nm over 3 min.

Statistical analyses

Three repetitions were performed to determine each value and their standard deviations. Data were analyzed using IBM SPSS Statistics 19.0 software (Ehningen, Germany) and presented as the means \pm standard deviations. The statistical significance was determined using Student's *t* test. The values were plotted using the means \pm standard errors (SEs) of the replications ($n = 3$). Values in figures marked with different lowercase and capital letters are significantly different at 0.05 and 0.01 probability levels, respectively.

Results

Cloning and structural features of *AhMCI*

AhMCI had a 1068-bp open reading frame, encoding a peptide of 355 amino acids, with a molecular weight and isoelectric point of 39,669.01 Da and 6.40, respectively. It contained five exons interrupted by four introns (Figs. S1 and 1), but no results were generated using PSORT software online to predict *AhMCI*'s subcellular localization. Transmembrane structures and a signal peptide analysis showed that *AhMCI* had no transmembrane helices nor a signal peptide, indicating that it should localize on the cytoplasmic matrix or organelle substrate. A comparison of the deduced *AhMCI* amino acid sequence with GenBank and EMBL databases revealed a high degree of conservation (Fig. S2).

As seen in Fig. S2, the *AhMCI* protein contained a putative conserved caspase-like catalytic domain peptidase C₁₄ p20 subunit (InterPro accession No. IPR001309) at the N-terminus and a non-catalytic p10 subunit (IPR002138) in the C-terminal domain. A region of 42 aa, which was shorter than that of AtMC4–9 in *A. thaliana*, linked the p20 and p10 subunits. Additionally, a lesion-simulating disease-1 (LSD1)-type domain was also found at the N-terminus, containing two CXXC-type zinc finger structures (IPR005735). LSD1, which encodes C₂H₂ zinc finger protein GATA-type



Fig. 1 Exon-intron structures of *AhMC1* gene. The exons are showed with orange boxes and introns by black lines. Numbers show the length of gene's exons and introns in bp

transcription factors, negatively regulated the hypersensitive response (Fig. S2). These features indicated that *AhMC1* belonged to the type I MC family defined by Fagundes et al. (2015).

Data obtained from the phylogenetic analysis of *AhMC1* using MEGA 6.0 software (Fig. 2) revealed two different types (I and II) in the phylogenetic tree. Type I consisted of 15 members, including *AhMC1*, *AtMC1–3* and *AdMC1*, while type II contained 6 proteins, *AtMC4–9*.

AhMC1 expression was induced by AI stress in peanut

The *AhMC1* protein has three forms: native form of approximately 39 KD and two activated forms of 19 KD and 17 KD, which could be detected at the same time (Martinon and Tschopp 2004). The expression of different forms of *AhMC1* protein occurred in the root tips of ZH2 and 99–1507 (Fig. 3). For ZH2, the

expression levels of the activated forms were greater than the native form (Fig. 3a and b). In contrast, the expression levels of the activated forms in 99–1507 were lower than the native form (Fig. 3c and d). As treatment time increased, the expression levels of all *AhMC1*-protein forms first increased and then decreased. In addition, the highest expression levels, which were 0.19, 3.57, and 3.15, respectively, occurred at 12 h after treatment (Fig. 3b). For 99–1507, the expression of the *AhMC1* protein showed an overall upward trend under AI-stress conditions (Fig. 3c). Significant differences were observed between AI-treated and control samples, with the native form reaching a maximum 0.36 at 24 h (Fig. 3d). Thus, the activated protein expression level in ZH2 at 12 h was significantly higher than in 99–1507 and the native form of the *AhMC1* protein in ZH2 was more easily cleaved and activated, thereby inducing PCD, compared with than in 99–1507 under AI-stress conditions.

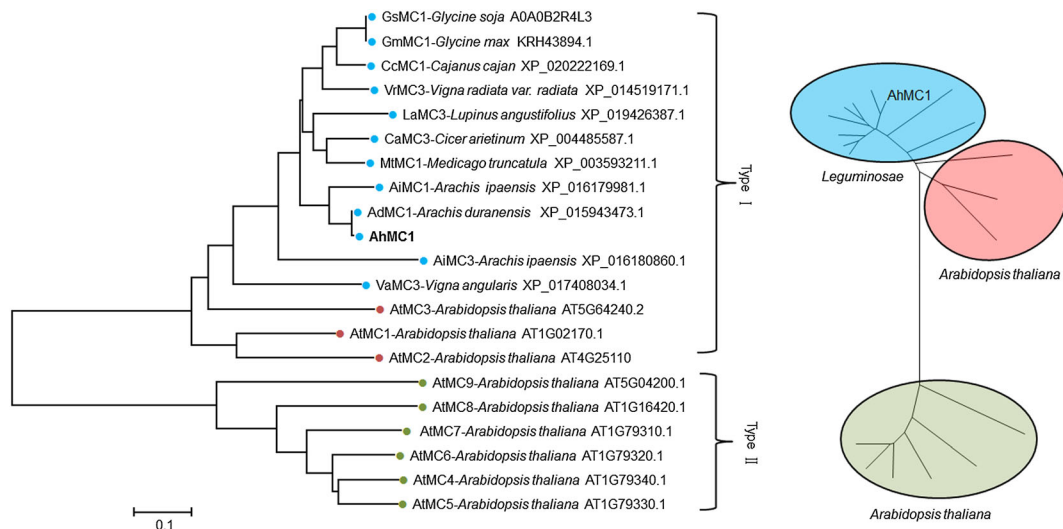


Fig. 2 Phylogenetic relationships of the metacaspase family proteins from peanut and other plant species. The phylogenetic tree was constructed using the Neighbor-Joining method using MEGA 6.0 software. The caspase gene *Casp1* (NM_009807.2) from *Mus musculus* was used as an outgroup to root the tree. Bootstrap values shown at the nodes were set to 1000 replicates, and branch lengths corresponding to the divergence of sequences are indicated by the relative scale (0.2 weighted sequence divergence). Two

groups were indicated. The acronym of metacaspase genes were named using the first letter of the genus followed by the first letter of the species: *AdMC*(*Arachis duranensis*) Metacaspase; *AhMC*(*Arachis hypogaea*); *AiMC*(*Arachis ipaensis*); *AtMC* (*Arabidopsis thaliana*); *CaMC* (*Cicer arietinum*); *CcMC*(*Cajanus cajan*); *GmMC* (*Glycine max*); *GsMC*(*Glycine soja*); *LaMC* (*Lupinus angustifolius*); *MiMC*(*Medicago truncatula*); *VaMC* (*Vigna angularis*); *VrMC*(*Vigna radiata* var. radiate)

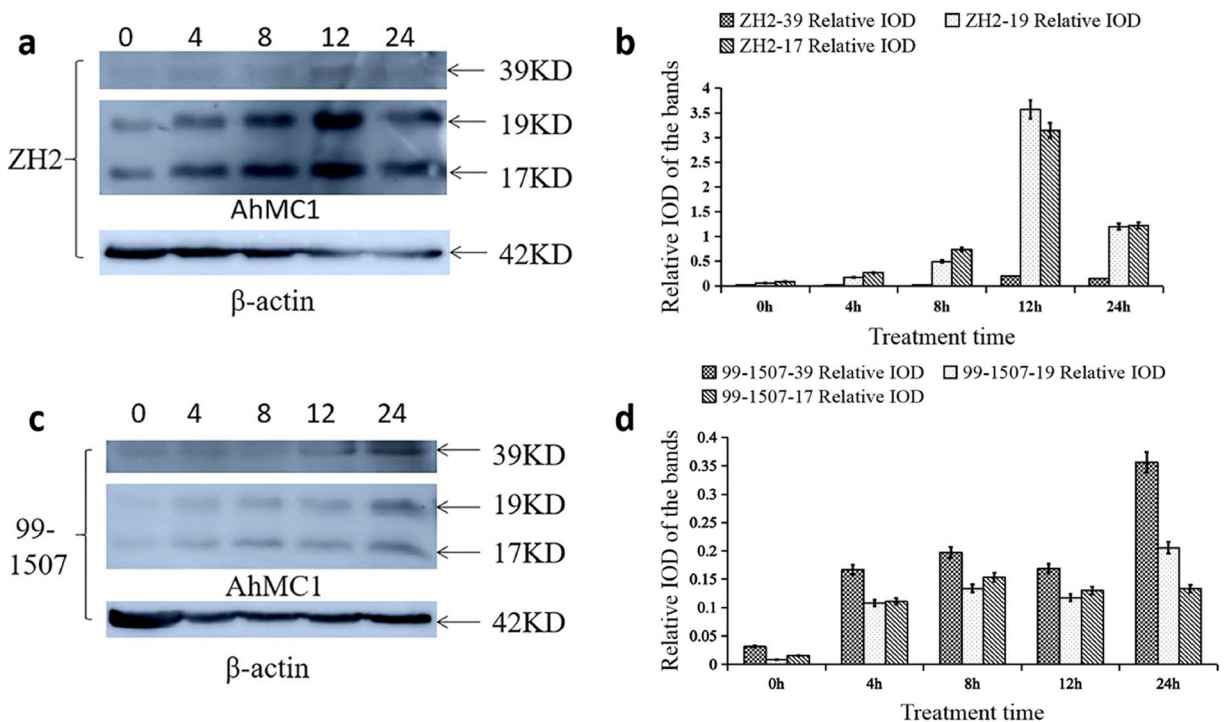


Fig. 3 Expression of *AhMC1* in ZH2 and 99-1507 cultivar under 100 μM AlCl_3 treatment for 0, 4, 8, 12, 24 h. **a**, Immunoblotting of ZH2; **b**, Relative IOD of the bands in ZH2; **c**, Immunoblotting of 99-1507; **d**, Relative IOD of the bands in 99-1507

Subcellular localization of AhMC1

AhMC1's subcellular localization changed as Al exposure time increased. Limited colloidal gold particles were found in the nuclear membranes of meristematic cells in peanut root tips not exposed to the Al stress, indicating that the synthesis of *AhMC1* protein was very low (Fig. 4a–c). Greater amounts of colloidal gold particles were distributed in the nuclear membranes after 4 h of the 100 μM AlCl_3 treatment (Fig. 4d). Likewise, limited colloidal gold particles were observed in both the cytoplasm and mitochondria under the same conditions, having disperse distributions (Fig. 4e). Moreover, a great amount of *AhMC1* was also observed in the nucleus, cytoplasm, mitochondria, and cell wall, with clustered distributions after 8 h of the Al treatment (Fig. 4f–h). However, after 24 h of treatment, there was less *AhMC1* protein in the mitochondria, but more *AhMC1* protein in the cytoplasm, indicating that the *AhMC1* protein transferred from mitochondria to cytoplasm and accumulated in the cytoplasm during Al stress (Fig. 4i and j). Limited gold particles appeared in nuclei and cell walls (Fig. 4i and j). The *AhMC1* polyclonal antibody was replaced by normal rabbit serum in the

negative control, revealing that no gold particles were located on mitochondria, cytoplasm, nucleus, cell wall, or other parts of meristematic cells (Fig. 4k and l).

Protein expression, purification and activity assay

A large amount of soluble *AhMC1* fusion protein was produced by inducing *E. coli* Rosetta (DE3) cells bearing pET-15b- *AhMC1* in LB liquid media with 0.5 mM isopropyl- β -D-thiogalactoside for 8 h at 20 °C. The purified *AhMC1* protein exhibited high caspase-3-like protease activity, which was much greater than that in the ZH2 root tip cells (Fig. 5).

Construction of transgenic tobacco plants

All the seedlings were produced following co-cultivation of WT calli with *Agrobacterium tumefaciens* carrying both *AhMC1* and *GFP* genes. PCR analysis and green fluorescence protein detection confirmed that *AhMC1* had been transformed into tobacco and stably inherited (Fig. 6). PCR indicated that 25 ST and 21 AT plants contained both the *AhMC1* and *GFP* genes (Fig. 6a). The transformation efficiencies were 83.33% for ST

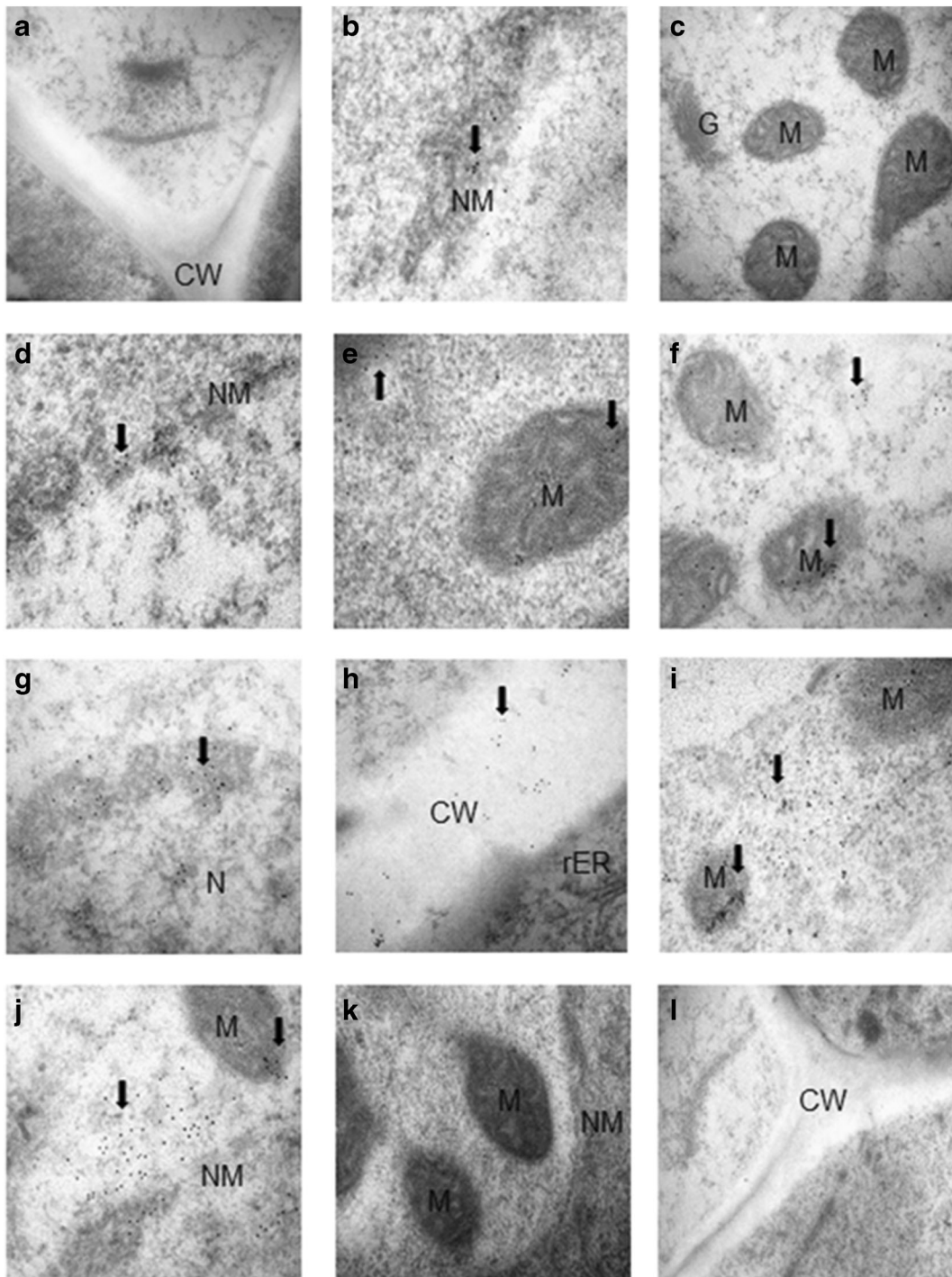


Fig. 4 Subcellular localization of AhMC1 by immune-electron microscopy in root tips of ZH2. **a-c**, 100 $\mu\text{mol/L}$ AlCl_3 treatment for 0 h (**a**: $\times 40,000$; **b-c**: $\times 60,000$); **d-e**, 100 $\mu\text{mol/L}$ AlCl_3 treatment for 4 h ($\times 60,000$); **f-h**, 100 $\mu\text{mol/L}$ AlCl_3 treatment for 8 h ($\times 60,000$); **i**, 100 $\mu\text{mol/L}$ AlCl_3 treatment for 12 h ($\times 60,000$); **j**,

100 $\mu\text{mol/L}$ AlCl_3 treatment for 24 h ($\times 60,000$); **k-l**, Negative control (**k**: $\times 60,000$; **l**: $\times 40,000$). Black arrows showing gold particles. N, Nucleus; NW, Nuclear membranes; CW, Cell wall; M, Mitochondria; G, Golgi apparatus; rER, Rough endoplasmic reticulum

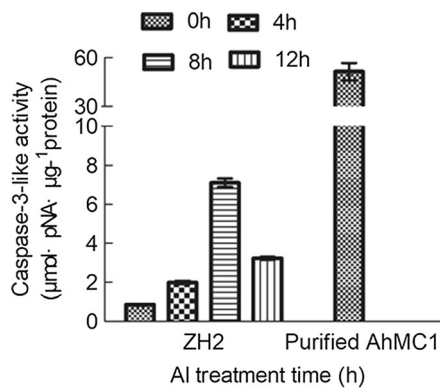
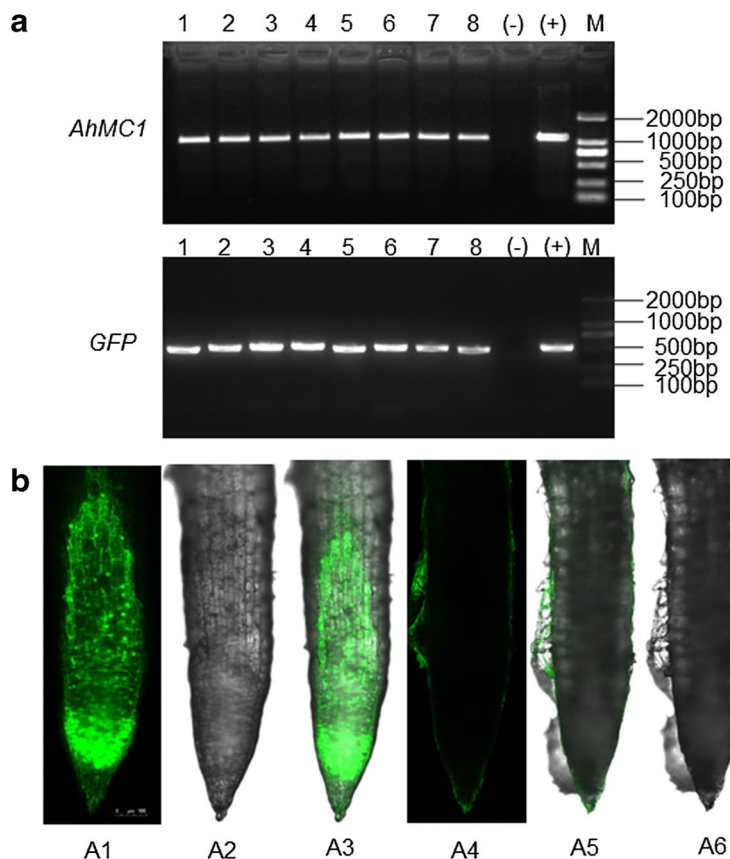


Fig. 5 The caspase-3-like protease activities in root tip cells of ZH2 and pET-15b-AhMC1 protein. Values are present as the mean \pm SD of three biological replications

plants and 70% for AT plants, respectively, based on Kan resistance (data not shown). The *GFP* gene in T1 transgenic and WT tobacco plants was observed under a confocal laser scanning microscope and revealed that only transgenic plants produced green fluorescence (A1 and A3, Fig. 6b).

Fig. 6 Identification of transgenic tobacco plants. **a.** Identification of AhMC1 and GFP gene by PCR. Lines from left to right: lanes 1–4, sense transgenic plants; lanes 5–8, antisense transgenic plants; lane (-), negative control (untransformed plants); lane (+), positive control (the Pbi121-AhMC1-eGFP plasmid); lane M, (DL2 000 marker). **b.** Green fluorescence detected in root tips of transgenic plants and the control by laser scanning confocal microscope. Bar = 100 μ m. A1: Fluorescent field of transgenic tobacco; A2: Bright field of transgenic tobacco; A3: Merge field of transgenic tobacco; A4: Fluorescent field of wild-type tobacco; A5: Bright field of wild-type tobacco; A6: Merge field of wild-type tobacco. Bar = 100 μ m



In addition, the phenotypic differences among WT, ST, and AT plants in T1 were analyzed. The plant types and fluorescence were almost similar among WT and ST, AT. Compared with WT, ST and AT plants had shorter petioles and smaller leaf blades, but there was not distinct difference between ST and AT (Fig. 7a and b).

AhMC1 enhanced Al-induced PCD by increasing the caspase-3-like activity

Caspase-3-like activities were monitored in this study to elucidate the function of AhMC1 accumulation. As shown in Fig. 7c, a significant increase in the caspase-3-like protease activities in root tips of WT, AT, and ST tobacco was observed after Al treatments. The caspase-3-like activity increased along with the Al concentration, but there were no obvious differences between the 100- and 200 μ M AlCl₃ treatments. The caspase-3-like activity in ST (5.27 μ mol·pNA· μ g⁻¹ protein) was significantly greater than those in AT (2.22 μ mol·pNA· μ g⁻¹ protein) and WT (3.53 μ mol·pNA· μ g⁻¹ protein) plants

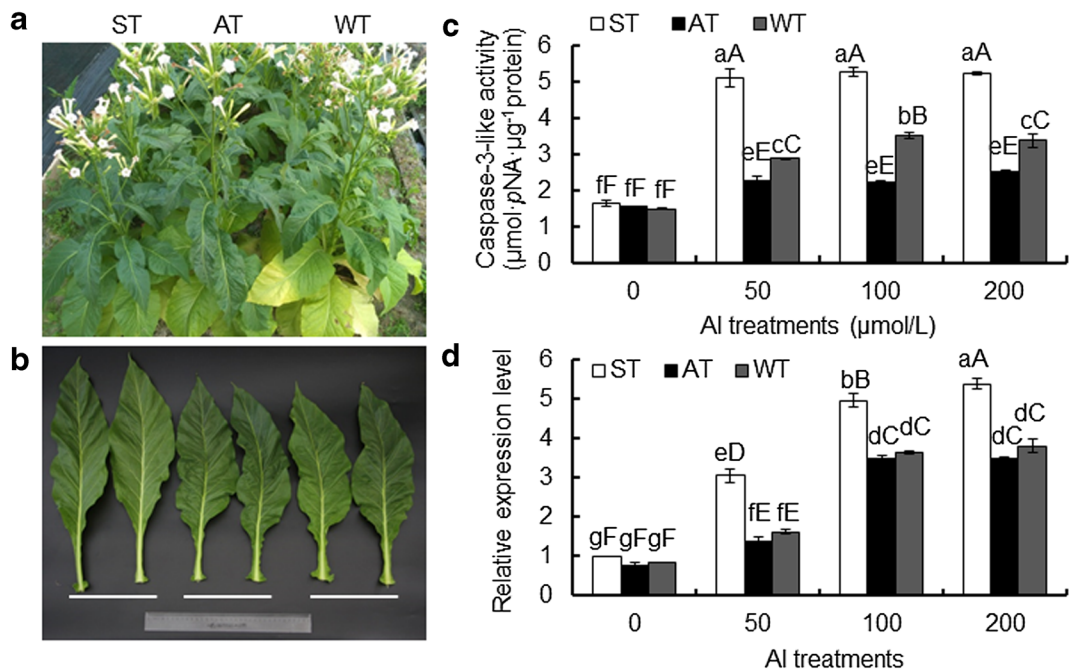


Fig. 7 The phenotype of transgenic (ST, sense transgenic, AT, antisense transgenic) and WT (wild type) tobacco in T1 generation. **a.** the whole plants; **b.** the leaves (from left to right: WT, ST,

AT); **c.** Caspase-3-like activity under Al treatments; **d.** Relative expression level under Al treatments

after 24-h 100 μM AlCl₃ treatment, which represented 3.21-, 1.44-, and 2.39- fold increases compared with the control (P value <0.01), respectively.

Likewise, the same change trend of *AhMCI* expression in ST, AT, and WT plants occurred with the same Al treatment (Fig. 7d). The expression of *AhMCI* increased more steadily and rapidly in root tips treated with greater Al concentrations in ST compared with AT and WT plants, and there was no remarkable difference between AT and WT plants receiving the same treatment (Fig. 7d). Thus, *AhMCI* appeared to enhance Al-induced PCD in peanut root tips, which may be triggered by an increased caspase-3-like activity.

Overexpression of *AhMCI* decreased resistance to Al stress

Al significantly inhibited root elongation in ST tobacco (Fig. 8a). Compared with the control, 50 μM Al could significantly inhibit the elongation of roots in ST plants, and the relative root elongation (RRE) was decreased by Al treatments. However, this Al treatment did not affect AT and WT plants. A 24-h treatment with 200 μM AlCl₃ produced RRE values in ST, AT, and WT of 58.07%, 66.52% and 66.22%,

respectively, compared with untreated plants (Fig. 8a). Thus, the overexpression of *AhMCI* decreased root elongation.

The integrity of the cell membrane during Al stress was evaluated using the nonpermeable dye, Evans blue. Al significantly increased the cell death of the membrane to differing degrees. Compared with the control, 50 μM AlCl₃ rapidly increased root tip cell death in ST plants, which was significantly greater than in AT and WT plants. When root tips were treated with 200 μM AlCl₃ for 24 h, there were up to 1.19- and 1.15- fold increases in the cell death in ST plants overexpressing *AhMCI* compared with AT and WT plants (Fig. 8b). Therefore, ST plants had greatly increased levels of cell death.

Al accumulation in root tips was detected using an inductively coupled plasma optical emission spectrometry technique. As shown in Fig. 8c, significant increases in Al accumulation in root tips were observed as Al concentrations increased, especially in ST plants. However, compared with AT and WT plants, the Al contents of ST plants were the greatest at the same concentrations. There were significant differences between ST and both AT and WT, but there was no significant difference between AT and WT plants.

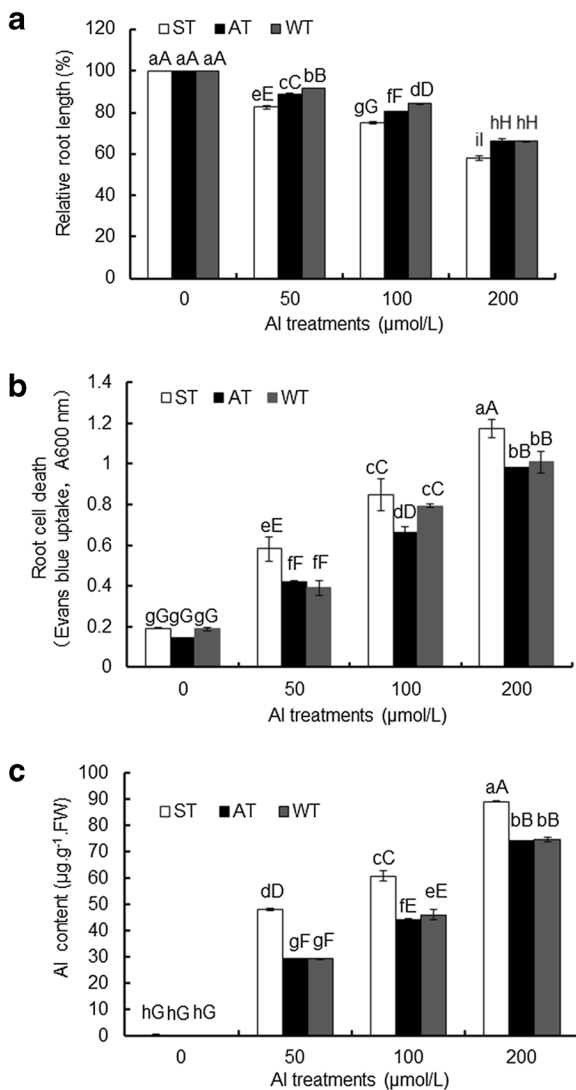


Fig. 8 Relative root length (a), root cell death (b), and Al content (c) in transgenic and WT tobacco plants under Al treatment

AhMC1 enhanced Al-induced PCD by changing the ROS capacity

To investigate the alteration in the redox status after Al treatments, the lipid peroxidation levels in root tips were assessed by measuring the MDA contents. There were no significant differences in the MDA content among ST, AT and WT not receiving an Al treatment. Significant changes in the lipid peroxidation level were observed initially after a 24-h 50 µM AlCl₃ treatment. The differences in the MDA contents in ST and WT plants was approximately 1.8-fold at 24 h after the 200 µM AlCl₃ treatment. Likewise, there was no significant

difference in the MDA contents of AT and WT under Al stress conditions (Fig. 9a). The activities of some antioxidant enzymes were monitored in this work to elucidate the function of AhMC1 accumulation in ST, AT and WT plants. The activities of SOD, POD, and CAT markedly and steadily increased along with the Al concentration compared with the control, but the degree of increase in ST plants was minimum (Fig. 9b–d). The transgenic ST plants showed significantly lower SOD, POD, and CAT activities than those of AT and WT plants after a 24-h 200 µM AlCl₃ treatment.

Discussion

MCs are widespread in the Viridiplantae and are divided into two types (I and II) based on amino acid sequence, which have similarities to metazoan “initiator” and “executioner” caspases, respectively (Hill and Nystrom 2015; Uren et al. 2000). In this study, the full-length of *AhMC1* in peanut was cloned and characterized. A sequence alignment analysis showed that the amino acid sequence of *AhMC1* had high homology with those from other species, especially *Leguminosae* family caspase-like proteases, and this indicated that *AhMC1* was a MC member. In *Arabidopsis*, both proline (AtMC1 and AtMC2) and glutamine (AtMC3) were enriched in predicted N-terminal prodomains, which represent upstream “initiator” caspases in mammals and might be responsible for protein–protein interactions between MCs and/or other signaling complexes, leading to subsequent MC activation (Vercammen et al. 2004). Fagundes et al. (2015) hypothesized that the acquisition of the zinc finger domain occurred later during MC gene family’s evolution, and they reported a distribution of 259 type I and 113 type II MCs in 42 plant species. The exon-intron structures in tomato (Liu et al. 2016b), rubber tree (Liu et al. 2016a), and rice (Wang and Zhang 2014) also supported type I MCs having greater intron numbers and short final exons in comparison with type II MCs. Here, the prodomain of *AhMC1* protein was enriched with proline, indicating that it might have similar function to those of AtMC1 and AtMC2 (Tsiatsiani et al. 2011). In conclusion, we hypothesize that *AhMC1* is a typical member of the type I MCs.

It is likely that MCs carry out various functions. In recent decades, some MC genes have been cloned and characterized, and PCD occurs in response to various

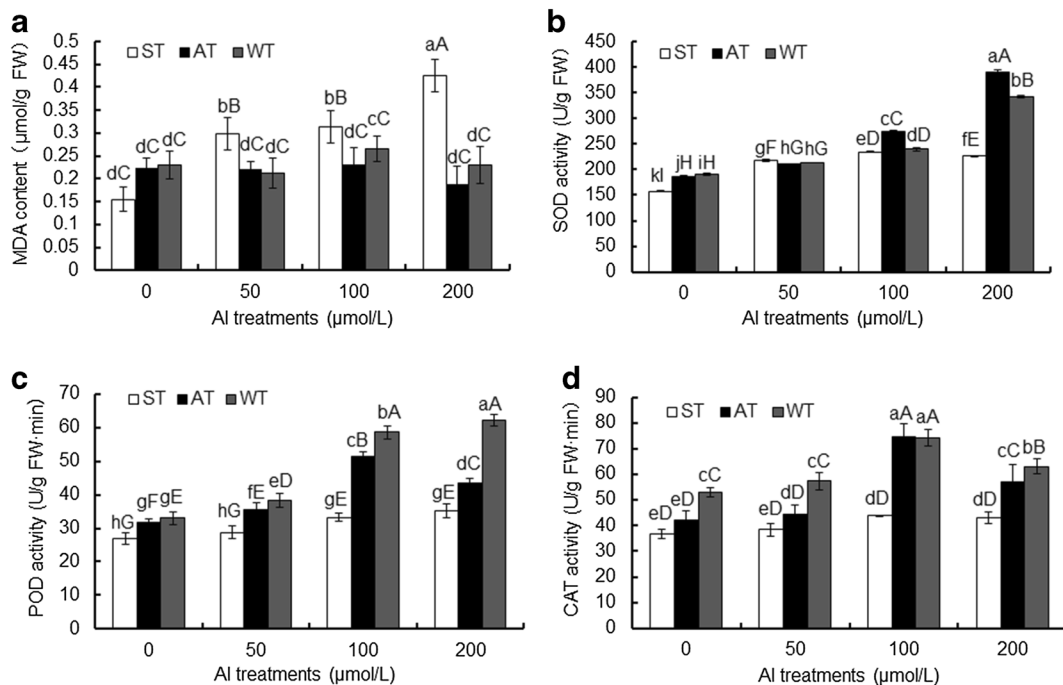


Fig. 9 Activities of MDA (a), SOD (b), POD (c) and CAT (d) in transgenic and WT tobacco plants under Al treatment

pathogens and elicitors, as well as abiotic stresses, in different species (Cao et al. 2012; Coll et al. 2014; Hao et al. 2016; Watanabe and Lam 2011; Wang et al. 2017b). The expression specificity of MCs in cells undergoing PCD was various in different tissues and organs of plants, such as *Arabidopsis*, rice, rubber tree, and grape (Kwon and Hwang 2013; Liu et al. 2016a; Wang and Zhang 2014). MCs became more active after the generation of signals leading to PCD, such as *BAX* expression, fungal pathogen attack (Wang et al. 2012), and ultraviolet light and H_2O_2 exposure (He et al. 2008). Liu et al. (2016b) showed that type I MCs (*MCI-6*) were significantly expressed in the roots of tomato during abiotic stress- or ethylene-induced PCD. In this study, *AhMCI* was highly expressed under Al-stress, and this was consistent with the expression levels of MCs in rice and tomato (Fig. 3a). Notably, the expression of *AhMCI* was in accordance with the occurrence of Al-triggered PCD and the activity levels of caspase-like proteases in peanut. Caspase-like proteases were activated during Al-induced PCD in peanut root tips, and there was a positive correlation between PCD and exposure time (Yao et al. 2016; Zhan et al. 2014). Therefore, we focused on the role of caspase-like proteases in Al induced PCD. MCs exhibit a caspase-3-like protease activity (Chai et al. 2017; Li and Franklin-Tong

2008; Tan et al. 2016; Wilkins et al. 2015). Here, there was a change between caspase-3-like protease activity and *AhMCI*'s expression level during Al-induced PCD, which further verified that *AhMCI* has a caspase-3-like protease activity. Additionally, the purified *AhMCI* protein which was expressed in *E. coli* Rossetta (DE3) cells also exhibited a high caspase-3-like protease activity (Fig. 5). Moreover, it is striking that both MC expression and caspase-like activity, possibly acting in the same signaling cascade, are required for effective PCD. Zhao et al. (2013) reported that the downregulation of *NtCYS*, a cystatin-regulating *NtCPI4*, or the overexpression of *NtCPI4*, a papain-like Cys protease, increased the caspase-like activity and caused premature PCD in tobacco. This suggests that *AhMCI* promotes PCD under Al-stress and is likely involved in the caspase-like protease signaling cascade.

Subcellular localization is critical in determining the mode of action for plant MCs. The subcellular localization of *AhMCI* during Al-induced PCD was examined. *AhMCI*'s subcellular localization changed as Al exposure time increased. Thus, the *AhMCI* protein may transfer from mitochondria to cytoplasm and accumulate in cytoplasm during Al-stress conditions. *Arabidopsis* MC9 was also present in the apoplast, nucleus, and cytoplasm, and its subcellular localization

changed during the late autolysis process (Bollhoner et al. 2013; Tsiatsiani et al. 2013). However, it was previously reported that OsMC5, -6, and -8 were exclusively localized in the cytoplasm without any localization in the nucleus (Huang et al. 2015). Our studies indicated that a potential cascade of cellular events occurs during Al-induced PCD via mitochondria-dependent pathways. Additionally, ROS is involved in regulating Al-induced PCD (Huang et al. 2014b). In this mechanism, including ROS bursts and caspase 3-like protease activity, AhMCI protein probably participated downstream of the signal transduction pathway. More studies need to be performed.

Overexpressing *AhMCI* in tobacco resulted in plants being less tolerant to Al stress. The T1 generation of *AhMCI* transgenic tobacco plants showed diverse resistance levels, which indirectly indicated a function for *AhMCI* gene in Al-stress responses as assessed by PCD indexes and physiological traits. Wang et al. (2009) reported that *Caenorhabditis elegans* apoptotic suppressor *Ced-9*, a *Bcl-2* homologue, inhibited both Al-induced PCD and Al-induced activity of caspase-like vacuolar processing enzyme, a crucial executioner of PCD, in tobacco. *Ced-9* significantly alleviated Al's inhibition of root elongation, decreased Al accumulation in the root tips, and greatly inhibited Al-induced gene expression in early responses to Al, leading to the enhanced Al tolerance of tobacco plants. There is also a negative correlation between Al-induced PCD and Al-resistance in peanut (Huang et al. 2014a; Zhan et al. 2013). Here, we showed that ST plants had shorter roots, and higher Al contents, as well as cell death, *AhMCI* expression, and caspase-3-like activity levels, than WT and AT plants under Al stress (Figs. 7c and d, 8a–c). A critical level of activated MC was needed to trigger Al-induced PCD, while in MC-overexpression plants this level was reached at a higher dose, which could promote the occurrence of PCD. The results indicate that *AhMCI* induces PCD as a trigger under Al stress.

MDA content was an indicator of the level of lipid peroxidation damage that resulted from oxidative stresses (Bailly et al. 1996). The MDA content of ST plants was significantly greater than those of AT and WT plants after Al treatments. This indicated that lipid peroxidation damage induced by Al was more serious in ST plants than in AT and WT plants. Al induces ROS bursts in mitochondria, which is an important component of the plant's reaction to toxic Al effects (Matsumoto and Motoda 2013). POD, CAT and POD activities treated

with high AlCl_3 (>100 μM) were significantly lower in ST plants than in WT plants (Fig. 9b–d), which indicated that the overexpression of *AhMCI* inhibited the antioxidant defensive reactions and affected the efficiency of the ROS scavenging system against ROS-mediated injury under Al stress. Additionally, the overexpression of *AhMCI* might have played a key role in improving ROS accumulation by inhibiting the activities of the SOD, POD, and CAT enzymes.

Acknowledgements This work was supported by the National Natural Science Foundation of China (Grant Nos. 31776190, 31560346, 31660350, 31701356, and 31860334), the Guangxi Natural Science Foundation of China (Grant No. 2016GXNSFBA380223), the Training Program for 1000 Young and Middle-aged Backbone Teachers of Guangxi Higher Education Institution in 2019.

Authors' contributions JZ and LFH conceived the general strategy; SCY, LSZ and CLP performed the experiments and analyzed the data; SZL and DX interpreted the results; AQW and WJX cultured the seedlings for experiments; SCY and SZL wrote the manuscript. JZ revised the manuscript. All the authors read and approved the final manuscript.

Compliance with ethical standards

Competing interests The authors declare that they have no conflict of interest.

References

- Acosta-Maspons A, Sepúlveda-García E, Sánchez-Baldoquín L, Marrero-Gutiérrez J, Pons T, Rocha-Sosa M, González L (2014) Two aspartate residues at the putative p10 subunit of a type II metacaspase from *Nicotiana tabacum* L. may contribute to the substrate-binding pocket. *Planta* 239:147–160
- Ahmad R, Zuily-Fodil Y, Passaquet C, Bethenod O, Roche R, Repellin A (2012) Ozone and aging up-regulate type II metacaspase gene expression and global metacaspase activity in the leaves of field-grown maize (*Zea mays* L.) plants. *Chemosphere* 87:789–795
- Bailly C, Benamar A, Corbineau F, Come D (1996) Changes in malondialdehyde content and in superoxide dismutase, catalase and glutathione reductase activities in sunflower seeds as related to deterioration during accelerated aging. *Physiol Plant* 97:104–110
- Bertioli DJ, Cannon SB, Froenicke L, Huang G, Farmer AD, Cannon EK, Liu X, Gao D, Clevenger J, Dash S, Ren L, Moretzsohn MC, Shirasawa K, Huang W, Vidigal B, Abernathy B, Chu Y, Niederhuth CE, Umale P, Araújo AC, Kozik A, Kim KD, Burow MD, Varshtey RK, Wang X, Zhang X, Barkley N, Guimarães PM, Isobe S, Guo B, Liao

- B, Stalker HT, Schmitz RJ, Scheffler BE, Leal-Bertioli SC, Xun X, Jackson SA, Michelmore R, Ozias-Akins P (2016) The genome sequences of *Arachis duranensis* and *Arachis ipaensis*, the diploid ancestors of cultivated peanut. *Nat Genet* 48:438–446
- Bollhoner B, Zhang B, Stael S et al (2013) Post mortem, function of *AtMC9* in xylem vessel elements. *New Phytol* 200:498–510
- Bozhkov PV, Suarez MF, Filonova LH, Daniel G, Zamyatnin AA Jr (2005) Rodriguez- executes programmed cell death during plant embryogenesis. *Proceedings of the National Academy of Sciences of the United States of America* 102:14463–14468
- Cao H, Cheng JJ, Liu CX, Li YY, Zou YM, Shu HR (2012) Detection of programmed cell death and cloning of caspase-like gene fragment from *Malus robusta* under drought stress. *Journal of Fruit Science* 29:525–529
- Chai L, Tudor RL, Poulter NS, Wilkins KA, Eaves DJ, Franklin FCH, Franklin-Tong VE (2017) MAP kinase PrMPK9-1 contributes to the self-incompatibility response. *Plant Physiol* 174:1226–1237
- Cheng PH, Lian S, Zhao R, Rao XM, McMasters KM, Zhou HS (2013) Combination of autophagy inducer rapamycin and oncolytic adenovirus improves antitumor effect in cancer cells. *Virology* 10:293–306
- Choi CJ, Berges JA (2013) New types of metacaspases in phytoplankton reveal diverse origins of cell death proteases. *Cell Death Dis* 4:e490–e497
- Coll NS, Vercammen D, Smidler A, Clover C, Van Breusegem F, Dangl JL, Epple P (2010) Arabidopsis type I metacaspases control cell death. *Science* 330:1393–1397
- Coll NS, Smidler A, Puigvert M, Popa C, Valls M, Dangl JL (2014) The plant metacaspase *AtMCI* in pathogen-triggered programmed cell death and aging: functional linkage with autophagy. *Cell Death & Differentiation* 21:1399–1408
- Escamez S, Andre D, Zhang B, Bollhoner B, Pesquet E, Tuominen H (2016) METACASPASE9 modulates autophagy to confine cell death to the target cells during *Arabidopsis* vascular xylem differentiation. *Biology Open* 5:122–129
- Fagundes D, Bohn B, Cabreira C, Leipelt F, Dias N, Bodanese-Zanettini MH, Cagliari A (2015) Caspases in plants: metacaspase gene family in plant stress responses. *Functional & Integrative Genomics* 15:1–11
- Gilio JM, Marcondes MF, Ferrari D, Juliano MA, Juliano L, Oliveira V, Machado MFM (2017) Processing of metacaspase 2 from *Trypanosoma brucei* (TbMCA2) broadens its substrate specificity. *BBA - Proteins and Proteomics* 1865:388–394
- Hao L, Goodwin PH, Hsiang T (2007) Expression of a metacaspase gene of *Nicotiana benthamiana* after inoculation with *Colletotrichum destructivum* or *Pseudomonas syringae* pv. Tomato, and the effect of silencing the gene on the host response. *Plant Cell Rep* 26(10):1879–1888
- Hao Y, Wang X, Wang K, Li H, Duan X, Tang C, Kang Z (2016) TaMCA1, a regulator of cell death, is important for the interaction between wheat and *Puccinia striiformis*. *Sci Rep* 6:26949–26960
- He R, Drury GE, Rotari V, Gordon A, Willer M, Farzaneh T, Woltering EJ, Gallois P (2008) Metacaspase-8 modulates programmed cell death induced by ultraviolet light and H₂O₂ in *Arabidopsis*. *J Biol Chem* 283:774–783
- Hill SM, Nystrom T (2015) The dual role of a yeast metacaspase: what doesn't kill you makes you stronger. *BioEssays* 37: 525–531
- Hoeberichts FA, ten Have A, Woltering EJ (2003) A tomato metacaspase gene is upregulated during programmed cell death in *Botrytis cinerea*-infected leaves. *Planta* 217:517–522
- Huang WJ, Oo TL, He HY, Wang AQ, Zhan J, Li CZ, Wei SQ, He LF (2014a) Aluminum induces rapidly mitochondria-dependent programmed cell death in Al-sensitive peanut root tips. *Bot Stud* 55:67–79
- Huang W, Yang X, Yao S, LwinOo T, He H, Wang A, Li C, He L (2014b) Reactive oxygen species burst induced by aluminum stress triggers mitochondria-dependent programmed cell death in peanut root tip cells. *Plant Physiology & Biochemistry* 82:76–84
- Huang L, Zhang H, Hong Y, Liu S, Li D, Song F (2015) Stress-responsive expression, subcellular localization and protein-protein interactions of the rice metacaspase family. *Int J Mol Sci* 16:16216–16241
- Kim SM, Bae C, Oh SK, Choi D (2013) A pepper (*Capsicum annuum* L.) metacaspase 9 (*Camc9*) plays a role in pathogen-induced cell death in plants. *Mol Plant Pathol* 14:557–566
- Kwon SI, Hwang DJ (2013) Expression analysis of the metacaspase gene family in *Arabidopsis*. *Journal of Plant Biology* 56:391–398
- Lam E, Zhang Y (2012) Regulating the reapers: activating metacaspases for programmed cell death. *Trends Plant Sci* 17:487–494
- Lema Asqui S, Vercammen D, Serrano I, Valls M, Rivas S, Van Breusegem F, Conlon FL, Dangl JL, Coll NS (2017) AtSERPIN1 is an inhibitor of the metacaspase AtMCI-mediated cell death and autocatalytic processing in plants. *New Phytol* 218:1156–1166
- Li S, Franklin-Tong VE (2008) Self-incompatibility in Papaver: a MAP kinase signals to trigger programmed cell death. *Plant Signal Behav* 3:243–245
- Liu H, Deng Z, Chen J, Wang S, Hao L, Li D (2016a) Genome-wide identification and expression analysis of the metacaspase gene family in *Hevea brasiliensis*. *Plant Physiology & Biochemistry* 105:90–101
- Liu H, Liu J, Wei Y (2016b) Identification and analysis of the metacaspase gene family in tomato. *Biochemical & Biophysical Research Communications* 479:523–529
- Martinon F, Tschopp J (2004) Inflammatory Caspases: linking an intracellular innate immune system to autoinflammatory diseases. *Cell* 117:561–574
- Matsumoto H, Motoda H (2013) Oxidative stress is associated with aluminum toxicity recovery in apex of pea root. *Plant Soil* 363:399–410
- Minina EA, Smertenko AP, Bozhkov PV (2014) Vacuolar cell death in plants. *Autophagy* 10:928–929
- Pan CL, Yao SC, Xiong WJ, Luo SZ, Wang YL, Wang AQ, Xiao D, Zhan J, He LF (2017) Nitric oxide inhibits Al-induced programmed cell death in root tips of Peanut (*Arachis hypogaea* L.) by affecting physiological properties of antioxidants systems and Cell Wall. *Front Physiol* 8:309–314
- Pena MS, Cabral GC, Fotoran WL, Perez KR, Stolf BS (2017) Metacaspase-binding peptide inhibits heat shock-induced death in *Leishmania amazonensis* (L.). *Cell Death and Disease* 8:e2645–e2654

- Phan TT, Sun B, Niu JQ, Tan QL, Li J, Yang LT, Li YR (2016) Overexpression of sugarcane gene SoSnRK2.1 confers drought tolerance in transgenic tobacco. *Plant Cell Rep* 35: 1–15
- Tan K, Wen C, Feng H, Chao X, Su H (2016) Nuclear dynamics and programmed cell death in *Arabidopsis* root hairs. *Plant Sci* 253:77–85
- Tsiatsiani L, Van Breusegem F, Gallois P, Zavalov A, Lam E, Bozhkov P (2011) Metacaspases. *Cell Death Differ* 18:1279–1288
- Tsiatsiani L, Timmerman E, Bock PJ, Vercammen D, Stael S, van de Cotte B, Staes A, Goethals M, Beunens T, Van Damme P, Gevaert K, Van Breusegem F (2013) The *Arabidopsis* METACASPASE9 Degradome. *Plant Cell* 25:2831–2847
- Uren AG, O'Rourke K, Aravind LA, Pisabarro MT, Seshagiri S, Koonin EV, Dixit VM (2000) Identification of paracaspases and metacaspases : two ancient families of caspase-like proteins, one of which plays a key role in MALT lymphoma. *Mol Cell* 6:961–967
- Vercammen D, Cotte BVD, Jaeger GD et al (2004) Type II Metacaspases *Atmc 4* and *Atmc 9* of *Arabidopsis thaliana* cleave substrates after arginine and lysine. *J Biol Chem* 279: 45329–45336
- Wang L, Zhang H (2014) Genomewide survey and characterization of metacaspase gene family in rice (*Oryza sativa*). *J Genet* 93:93–102
- Wang W, Pan J, Zheng K, Chen H, Shao H, Guo Y, Bian H, Han N, Wang J, Zhu M (2009) Ced-9 inhibits Al-induced programmed cell death and promotes Al tolerance in tobacco. *Biochemical & Biophysical Research Communications* 383: 141–145
- Wang X, Wang X, Feng H, Tang C, Bai P, Wei G, Huang L, Kang Z (2012) TaMCA4, a novel wheat metacaspase gene functions in programmed cell death induced by the fungal pathogen *Puccinia striiformis* f. sp. *tritici*. *Mol Plant-Microbe Interact* 25:755–764
- Wang C, Lü P, Zhong S, Chen H, Zhou B (2017a) LcMCII-1, is involved in the ROS-dependent senescence of the rudimentary leaves of *Litchi chinensis*. *Plant Cell Rep* 36:89–102
- Wang Y, Liu X, Tao L, Xu P, Gao X, Li H, Yang Z, Wu W (2017b) Expression and immunogenicity of VP40 protein of ZEBOV. *Archives of Iranian Medicine* 20:246–250
- Watanabe N, Lam E (2005) Two *Arabidopsis* metacaspases AtMCP1b and AtMCP2b are arginine/lysine-specific cysteine proteases and activate apoptosis-like cell death in yeast. *J Biol Chem* 280:14691–14699
- Watanabe N, Lam E (2011) *Arabidopsis* metacaspase 2d is a positive mediator of cell death induced during biotic and abiotic stresses. *Plant J* 66:969–982
- Wilkins KA, Bosch M, Haque T, Teng N, Poulter NS, Franklin-Tong VE (2015) Self-incompatibility-induced programmed cell death in field poppy pollen involves dramatic acidification of the incompatible pollen tube cytosol. *Plant Physiol* 167:766–779
- Wrzaczek M, Vainonen JP, Stael S et al (2015) GRIM REAPER peptide binds to receptor kinase PRK5 to trigger cell death in *Arabidopsis*. *EMBO J* 34:55–66
- Yao SC, Huang WJ, Pan CL, Zhan J, He LF (2016) Caspase-like proteases regulate aluminum-induced programmed cell death in peanut. *Plant Cell Tissue & Organ Culture* 127:691–703
- Yao SC, Zhan J, Pan CL, Xiong WJ, Xiao D, Wang YL, Shen H, Wang AQ, He LF (2019) Identification and validation of reference genes for real-time qPCR normalization during Al-induced programmed cell death in peanut. *Biol Plant* 63: 237–246
- Zhan J, He HY, Wang TJ, Wang AQ, Li CZ, He LF (2013) Aluminum-induced programmed cell death promoted by *AhSAG*, a senescence-associated gene in *Arachis hypogaea* L. *Plant Sci* 210:108–117
- Zhan J, Li W, He HY, Li CZ, He LF (2014) Mitochondrial alterations during Al-induced PCD in peanut root tips. *Plant Physiology & Biochemistry* 75:105–113
- Zhang C, Gong P, Wei R, Li S, Zhang X, Yu Y, Wang Y (2013) The metacaspase gene family of *Vitis vinifera* L.: characterization and differential expression during ovule abortion in stenospermocarpic seedless grapes. *Gene* 528:267–276
- Zhao P, Zhou XM, Zhang LY, Wang W, Ma LG, Yang LB, Peng XB, Bozhkov PV, Sun MX (2013) A bipartite molecular module controls cell death activation in the basal cell lineage of plant embryos. *PLoS Biol* 11:e1001655–e1001670

Publisher's note Springer Nature remains neutral with regard to jurisdictional claims in published maps and institutional affiliations.